Water Splitting

DOI: 10.1002/anie.201203174

p-Type InP Nanopillar Photocathodes for Efficient Solar-Driven Hydrogen Production**

Min Hyung Lee, Kuniharu Takei, Junjun Zhang, Rehan Kapadia, Maxwell Zheng, Yu-Ze Chen, Junghyo Nah, Tyler S. Matthews, Yu-Lun Chueh, Joel W. Ager, and Ali Javey**

Water splitting by using sunlight for the production of hydrogen yields a storable product, which can be used as a fuel.[1,2] There is considerable research into H_2 generation, namely the reduction of protons to H_2 in aqueous solution using semiconductor photocathodes.[3,4] To maximize the photoelectrochemical (PEC) performance, the selection of the active materials and device configurations should be carefully considered. First, the short-circuit current density (J_{sc}) should be maximized by choosing materials with high optical absorption coefficients and low carrier recombination rates,[5] both in the bulk and at the surface. The reflectance should be minimized by using surface nanotexturing to further improve light absorption.[6–8] The onset potential (E_{os}) of the PEC device versus the reversible H^+/H_2 redox potential should be maximized. Finally, the surface energy needs to be controlled to minimize the accumulation of gas bubbles on the surface of the photoelectrode. Light absorbers with band gaps in the range of 1.1–1.7 eV provide both a good match to the terrestrial solar spectrum and a significant fraction of the 1.23 eV free energy required to split water. Overpotentials associated with the electron transfer to (solvated) protons in aqueous solution should be minimized by improving carrier transport from semiconductor to electrolyte by decorating the semiconductor with cocatalysts, tuning band edges, and decreasing contact resistance.

p-Type Si has been extensively investigated as a photocathode for photochemical hydrogen production. Planar Si has relatively low short-circuit current densities under AM1.5 G illumination, approximately 10 mA cm^{-2} (reference [9]), compared to what can be achieved in a pn junction solar cell (> 35 mA cm^{-2}).[10] Nanostructuring and incorporation of cocatalysts have been used to raise the short-circuit current density to over 30 mA cm^{-2}.[11,12] A recent study using n^+p Si radial junction microwires reported an E_{os} value of 0.54 V and an J_{sc} value of 15 mA, leading to an overall efficiency near 6%.[13] The onset potential observed to date for p-Si photocathodes is less than half of the value required for overall water splitting (1.23 V). This low onset potential limits the performance of tandem or "Z-scheme" approaches, which would function without external bias, as it limits the potential overlap required for spontaneous water splitting.[14,15] An ideal photocathode for use in a solar-driven hydrogen production system without bias should have both a high current density and a favorable open-circuit potential versus the reversible H^+/H_2 redox couple.

Herein, we employ nanotextured p-InP photocathodes in conjunction with a TiO_2 passivation layer and a Ru cocatalyst to increase both J_{sc} and E_{os} values under H_2 evolution conditions. InP has a number of attractive attributes as a photocathode: 1) Its band gap of 1.3 eV is well-matched to the solar spectrum; InP-based solar cells have achieved AM1.5 G efficiencies of up to 22%.[16] 2) The conduction band edge of InP is slightly above the water reduction potential, thus electron transfer is favorable in this system. 3) The surface-recombination velocity of untreated InP is low (ca. 10^4 cm s^{-1} for n-type and 10^5 cm s^{-1} for p-type),[17] which is particularly important for nonplanar devices with high surface areas, such as those explored in this study. For these reasons, InP has been studied previously as a photocathode for both water splitting and CO_2 reduction.[18–20] Specifically, Heller and Vadimsky reported attractive PEC performances with current densities up to 28 mA cm^{-2} and conversion efficiencies of approximately 12% in InP photocathodes.[19] Motivated by these results, we use InP as a model material system to elucidate the role of surface nanotexturing on the PEC device performance. We find that nanotextured InP photocathodes exhibit drastically enhanced performances compared to our planar cells that were processed using identical conditions. We examine the various effects of nanotexturing

[*] M. H. Lee,[+] K. Takei, J. Zhang, R. Kapadia, M. Zheng, J. Nah,[++] J. W. Ager, Prof. A. Javey
Material Sciences Division, Lawrence Berkeley National Laboratory
Berkeley, CA 94720 (USA)
E-mail: jwager@lbl.gov
ajavey@berkeley.edu
M. H. Lee,[+] K. Takei, J. Zhang, R. Kapadia, M. Zheng, J. Nah,[++] Prof. A. Javey
Electrical Engineering and Computer Sciences
University of California, Berkeley, CA 94720 (USA)
M. H. Lee,[+] T. S. Matthews, J. W. Ager, Prof. A. Javey
Joint Center for Artificial Photosynthesis
Lawrence Berkeley National Laboratory, Berkeley, CA 94720 (USA)
Y.-Z. Chen, Y.-L. Chueh
Material Sciences and Engineering
National Tsing-Hua University, Hsinchu 30013 (Taiwan)
[+] Current address: Department of Applied Chemistry
Kyung Hee University, Yongin, Gyeonggi 446-701 (Korea)
[++] Current address: Electrical Engineering
Chungnam National University, Daejeon, 305-764 (Korea)

[**] The materials preparation and device fabrication were supported by Berkeley Sensor and Actuator Center. The material and device characterizations were performed in the Joint Center for Artificial Photosynthesis, a DOE Energy Innovation Hub, supported through the Office of Science of the U.S. Department of Energy under Award Number DE-SC0004993. A.J. acknowledges a Sloan Research Fellowship and support from the World Class University program at Sunchon National University.

Supporting information for this article is available on the WWW under http://dx.doi.org/10.1002/anie.201203174.

© 2012 Wiley-VCH Verlag GmbH & Co. KGaA, Weinheim

on the device performance, including light management, surface area, wettability, and surface potential. The findings allow a direct comparison of devices with planar and nanotextured InP by using the same starting substrate, identical steps for processing, and the same measurement setups for characterization.

Figure 1a depicts the fabrication process scheme for making InP nanopillars (NPLs). p-InP (100) bulk wafers with a Zn doping concentration of approximately $5\times10^{17}\,cm^{-3}$ were coated with approximately 25 nm of poly(methyl methacrylate) (PMMA) and treated in a reactive ion etching (RIE) process. A $CH_4/H_2/Ar$ mixture was used as the RIE processing gas at a radio-frequency (RF) power of 150 W. During the 30 min etching process, PMMA partially decomposes, thereby forming amorphous carbon islands, which function as a nanopatterning mask, without the use of any lithographic processes. After completion of the RIE step, O_2 plasma treatment and a two-minutes wet-etching step in HCl/H_3PO_4 (3:1) were used to remove the surface-damaged layers and contaminants. The resulting InP NPLs are conical (diameters—top: 15 nm, bottom: 130 nm), approximately 400 to 600 nm tall, and have an average pitch of approximately 250 nm (Figure 1b). Next, a TiO_2 passivation layer was deposited on the InP NPLs using atomic-layer deposition (ALD) to enhance the stability of the devices, and then a thin film of Ru cocatalyst (thickness ca. 2 nm) was sputtered on the surface. The final device configuration of InP NPL PEC cells is depicted in Figure 1b inset. Figure 1c–e shows the transmission electron microscope (TEM) images of the InP NPLs. From the high resolution TEM image (Figure 1e) and the corresponding diffraction pattern, the single-crystalline structure of the InP NPLs coated with amorphous TiO_2 and Ru layers is clearly evident. The planar devices were processed using the identical process scheme and using the same starting p-InP substrate described above, except that RIE was not performed on the surface.

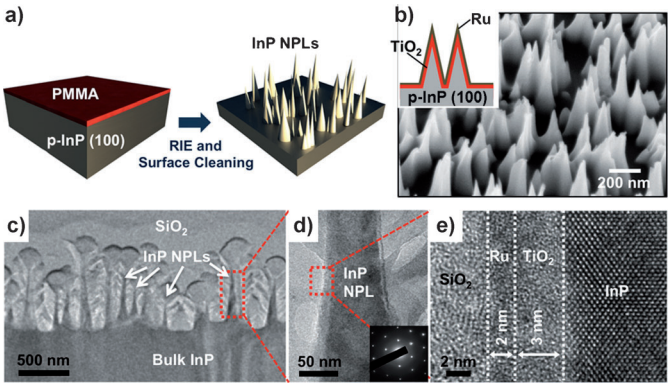

Figure 1. a) Process flow for fabrication of InP nanopillar arrays. b) SEM iamge of the resulting NPL arrays. Inset shows the schematic of a PEC cell made of p-InP NPLs, a TiO_2 passivation layer (thickness, 3–5 nm), and the Ru cocatalyst (thickness, ca. 2 nm). c–e) TEM images of p-InP NPLs coated with TiO_2/Ru layers. Note that for TEM sample preparation and imaging purposes, the surface of the substrate is coated with a thick layer of evaporated SiO_x. The inset in (d) shows diffraction patterns confirming the crystalline structure of InP NPLs.

It is important to assess the surface quality of fabricated InP NPLs after RIE and surface-treatment processes. Photoluminescence (PL) spectra of a p-InP substrate with and without RIE processing, corresponding to NPL and planar geometries, respectively, were recorded using an excitation wavelength of 632 nm (Figure 2a). The PL intensity and line width are nearly identical for both samples, thus suggesting that the optoelectronic properties of InP is preserved during RIE and post-treatment processes. Time-resolved PL (TRPL) measurements with an excitation wavelength of 800 nm were performed to extract the minority carrier life time of the NPL and planar samples (Figure 2b). From the TRPL data, at a PL intensity of 1/e, decay times of approximately 1.7 and 1.4 ns were extracted for the planar and NPL samples, respectively. The TRPL data illustrate that the NPL fabrication process does not significantly decrease the minority carrier lifetime. It should be noted that the absorption length in InP for incident photons with wavelengths of 632–800 nm is approximately 170–300 nm based on the bulk absorption coefficients. Although the filling factor of the NPLs is lower than 50%, this short absorption length as compared to the NPL height ensures that most of the PL signal arises from the NPLs rather than the bulk substrate.

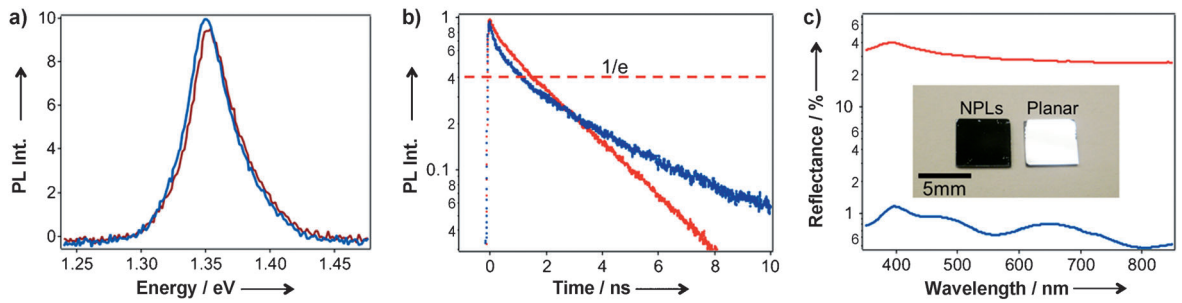

Figure 2. a) Room-temperature PL spectra of planar (red trace) and NPL (blue) InP samples (without TiO_2 and Ru surface layers). The excitation wavelength is 633 nm. b) Time-resolved PL measurements of planar (red spectrum) and NPL (blue) samples. The monitoring wavelength is 922 nm with an excitation wavelength of 800 nm. c) Specular reflectance of planar (red trace) and NPL (blue) substrates demonstrating the drastically reduced optical reflectivity of the NPLs as clearly evident from visual inspection (inset). The y-axes in (b) and (c) have a logarithmic scale.

© 2012 Wiley-VCH Verlag GmbH & Co. KGaA, Weinheim

The specular reflectances of the planar and NPL samples in the wavelength range of 300–900 nm are shown in Figure 2c. As expected, the reflectance of InP NPL structures (ca. 1% reflectance) is drastically reduced compared to the planar InP wafer (ca. 30% reflectance). The low reflectance of conical NPL arrays is attributed to the suppressed Fresnel reflection owing to the surface texture, which acts as a homogeneous medium with an intermediate refractive index between air (and/or liquid) and the semiconductor.[21] The drastically reduced reflectance of NPL arrays is also evident in the optical photographs of the samples (Figure 2c inset) with the NPL sample appearing black.

Photoelectrochemical measurements were performed using a conventional three-electrode configuration with an Ag/AgCl (saturated KCl) reference electrode and Pt counter electrode in $HClO_4$ (1M, pH 0.51) electrolyte. AM1.5 G illumination was provided by a solar simulator (Solar Light); the incident power (100 mW cm^{-2}) was calibrated with a pyranometer. To enable a comparison to literature, the reference voltage was converted from Ag/AgCl (saturated KCl) to the normal hydrogen electrode (NHE) using $E_{NHE} = E_{Ag/AgCl} + 0.198$ V. Initial measurements were performed without any cocatalyst. However, we found that a sputter-deposited 2 nm layer of Ru catalyst improved the open-circuit potential of InP cathodes by approximately 0.5 V, although the photocurrent density level remained similar (Figure S1 in the Supporting Information). Therefore all data included herein was obtained with the Ru cocatalyst (thickness, 2 nm).

TiO_2 passivation has been used in the past to improve the stability of Cu_2O and Si photoanodes under basic conditions;[22,23] here we employ this technique to improve the stability of InP in an acidic medium. Stable photocathodes were formed by using a thin layer (2–5 nm) of TiO_2, which was conformably coated on InP substrates (both planar and NPLs) by using ALD, followed by a layer of 2 nm of sputtered Ru. In the high resolution TEM image of a TiO_2-coated NPL sample (Figure 1e) it can be seen that the interface between the InP and the conformal TiO_2 is well-defined. We found that a 5 nm TiO_2 layer was optimal in terms of protecting the InP surface while not adversely affecting the PEC performance. A photocathode consisting of p-InP NPLs coated by 5 nm of TiO_2 and 2 nm of Ru operates for more than four hours at a stable cathodic photocurrent of approximately 37 mA cm^{-2} (Figure 3a). The SEM images in Figure S2 in the Supporting Information also show that the shape and morphology of the TiO_2-protected NPLs remain unchanged after PEC measurements. The results clearly indicate the high stability of the InP NPL photocathodes. TiO_2 coating also improved the stability of the planar InP, but there was a decline from an initial value of 27 to less than 18 mA cm^{-2} after four hours. The performance decline for planar InP, however, coincides with the visual observation of an excess amount of H_2 bubbles accumulating on the planar InP surface; these bubbles interfere with the diffusion of the electrolyte to the photocathode (Figure 3b). In contrast, H_2 gas molecules do not stick to the surface of the InP NPLs and desorb quickly from the surface owing to the low surface energy of the InP NPLs (Figure 3c). The improved H_2 desorption is an important

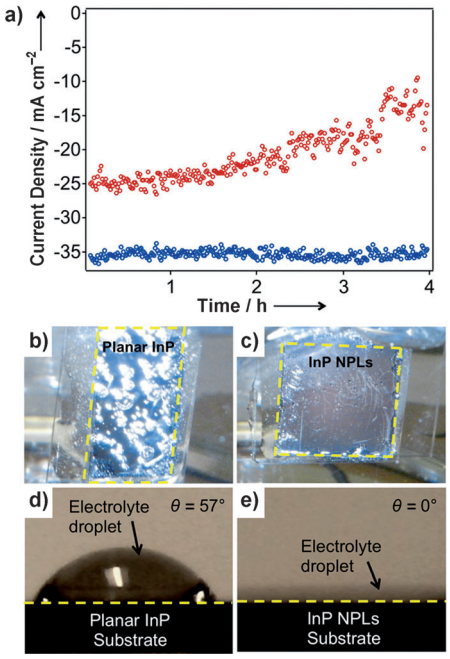

Figure 3. a) Long-term stability test of the photocurrent level of a p-InP/TiO_2/Ru photocathode in $HClO_4$ (1 M) for both planar (red circles) and NPL (blue) samples. The applied potential was 0.23 V (vs. NHE). b, c) Optical images depicting the effect of H_2 bubble formation on the surfaces of the planar and NPL samples, respectively, during PEC measurements. d, e) Surface contact angles of $HClO_4$ (1 M) droplets on p-InP/TiO_2 samples with a planar (d) and an NPL (e) platform.

advantage of the nanotextured surfaces with controlled surface wetting properties. Specifically, the measured contact angle of $HClO_4$ (1M) electrolyte droplets on planar InP (θ = 57°) is larger than that of InP NPLs (θ = 0°; Figure 3d,e). The use of surfactants for removal of bubbles on PEC devices was reported, however, surfactants can be readily reduced or oxidized during the measurements.[12] Instead of surfactants, the nanotexturing of surfaces reported herein can be beneficial for enhancing the cell efficiency by reducing adverse effect of H_2 bubbles. Notably, given the enhanced wetting properties of the InP NPL arrays, the overpotential may also be reduced compared to planar InP samples owing to the formation of a more intimate electrolyte–semiconductor interface.

Figure 4a shows the PEC performance of p-InP photocathodes with planar and NPL configurations. Here, the surface is coated with 5 nm of TiO_2 and 2 nm Ru cocatalyst. The NPL cell shows a higher current density (ca. 37 mA cm^{-2}) than our planar InP (ca. 27 mA cm^{-2}) owing to the increased absorption of above band gap photons. This high current density for NPLs is at the theoretical limit given the band gap of InP.[24] Note that while the AM1.5 G simulated solar spectrum used here was calibrated with a reference diode, an uncertainty in the exact spectrum and small variation between different setups always exist. In this regard, we used identical measurement setups for both planar and NPL samples to elucidate the effect of nanotexturing on the PEC device performance. The observed E_{os} value of 0.73 V (vs. NHE) and J_{sc} of 37 mA cm^{-2} for NPLs are comparable to state-of-the-art

© 2012 Wiley-VCH Verlag GmbH & Co. KGaA, Weinheim

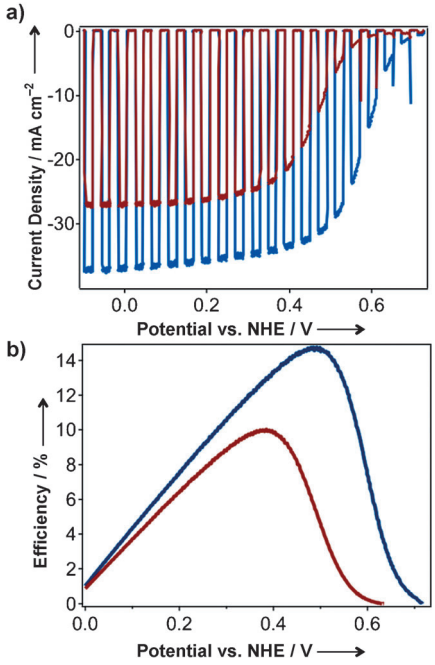

Figure 4. PEC performance of p-InP photocathodes. a) *J–E* data for planar (red trace) and NPL (blue) samples measured in $HClO_4$ (1 M, pH 0.51) under chopped illumination. b) Corresponding photon–energy conversion efficiency calculated by using Equation (1) for planar (red trace) and NPL (blue) samples.

InP homojunction solar cells (AM0, $J_{sc} = 34\ mA\,cm^{-2}$, $E_{os} = 0.87$ V).[25] Notably, the photocurrent from InP NPLs was generated at a more positive potential (0.73 V vs. NHE) compared to the planar InP (0.5 V vs. NHE). The improved onset potential could be attributed to a combination of factors that are explained later herein. The overall performance of the planar cells that were fabricated using our process schemes are lower than those reported by Heller and Vadimsky[19] This comparison suggests that additional improvement in the efficiency of the planar and NPL cells may be possible in the future through further process optimization.

We note that in previous reports, Si nano/micro wires have shown favorable onset potentials E_{os}, but lower current densities compared to planar Si.[13] The lower current density might be due to the carrier recombination loss from increased surface area of Si wire arrays. In contrast to those reports, InP NPLs show favorable E_{os} values with increased current density over planar InP owing to the low surface recombination velocity of carriers in InP, even without surface treatment as depicted from TRPL measurements (Figure 2b).

Overall PEC performance was evaluated by computing the photon-to-energy conversion efficiency of the PEC cell (η_{cell}) according to the following equation,[26]

$$\eta_{cell} = \left(\frac{E_{in} - E_{out}(H^+/H_2)}{I_0}\right)100\% \qquad (1)$$

where I_0 (100 $mW\,cm^{-2}$ for this study) is the impinging light power, E_{in} is the applied bias vs. NHE, and $E_{out}(H^+/H_2)$ is the voltage of the redox couple vs. NHE, in this case $E_{out}(H^+/H_2) = -0.03$ V. This equation assumes an ideal Pt counter electrode with no overpotential losses for water oxidation.[27] The maximum H_2 production efficiency for the p-InP NPLs reaches approximately 14% at an applied bias relative to a perfect anode of approximately 0.5 V (Figure 4b). This efficiency value exceeds that of our planar control sample that was processed by using identical steps and measured using the same setup; the planar sample exhibits a maximum efficiency of approximately 9% (Figure 4b).

In our InP/TiO_2/Ru photocathodes, p-InP serves as the absorber layer. Photogenerated electrons in InP are transported to the n-TiO_2 interface owing to band bending. The TiO_2 layer is too thick (2–5 nm) for the electrons in InP to tunnel through an expected barrier that arises from the conduction-band mismatch of InP/TiO_2. Instead, we speculate that electrons are transported through the amorphous TiO_2 through tail or defect states. Pinholes may also contribute to the transport of electrons through the thin TiO_2 layers. Subsequently electrons are consumed in a redox reaction at the electrolyte interface with the help of Ru cocatalysts. The enhanced efficiency of the NPLs arises from a combination of increased current density and onset potential E_{os}. Given the improved photon management properties of the NPLs with reduced optical reflectance (Figure 2c), the increased current density is expected to be the reason for the enhanced efficiency of the NPLs. The cause of the observed E_{os} enhancement for the NPLs, however, is less clear. Three effects may contribute to this trend: 1) NPLs have a higher photoelectrode–electrolyte junction area compared to planar devices for the same sample size. As a result, NPLs exhibit a lower overpotential owing to lower local current density compared to the planar substrate. A similar hypothesis was reported for Si photocathodes.[28] Moreover, the higher wettability of the electrolyte on the NPL InP surfaces (Figure 3d,e) could lower the overpotential compared to planar surfaces owing to an improved electrode–electrolyte interface. 2) Possible surface n-doping of NPLs and surface state passivation[29] is induced by the RIE process. Incorporation of carbon atoms into the surface along with hydrogen passivation of Zn acceptor atoms near the surface by RIE[29] can induce an ultrashallow n-doping of the InP NPL surface. Moreover, phosphorous atoms can be removed from the surface during RIE, thereby resulting in the formation of an electron-rich layer owing to the donor-like behavior of phosphorous vacancies.[30] This effect was elucidated by Mott–Schottky measurements (Figure S3 in the Supporting Information), where a shift of approximately 70 mV in the flat band potential is observed for NPL samples compared to the planar samples. As a result, a more favorable surface band bending is obtained in RIE-processed InP NPLs. 3) NPLs have different exposed surface orientations compared to the planar (100) wafers; these might have superior electron-transfer and surface-chemistry characteristics.[31] However, the crystal orientation effect is not expected to be dominant in the system explored here, because the InP surface is coated with an amorphous TiO_2 layer. Overall, the onset-potential improvement for InP NPLs is expected to be a combination of

 © 2012 Wiley-VCH Verlag GmbH & Co. KGaA, Weinheim

the various effects described above with the first two mechanisms playing a more dominant role.

In summary, p-InP NPL arrays were fabricated by a simple self-masking RIE process, and approximately 14% energy conversion efficiency was achieved with a Ru cocatalyst. High stability is obtained by passivating the surface with 3–5 nm of TiO_2 deposited by ALD. PL and TRPL measurements show that the high optical quality of InP is preserved during the NPL fabrication process. Compared to the planar controls, the NPL arrays exhibit drastically improved solar-driven hydrogen generation. Specifically, higher current densities approaching the theoretical limit and more favorable onset potentials are observed through surface nanotexturing. Furthermore, the lowered surface energy of the NPLs results in fast desorption of H_2 bubbles from the surface of InP; this property yet presents another important characteristic of an efficient PEC device. In the future, the reported NPL fabrication process and PEC device architecture can be applied to thin film InP (ca. 1 μm thick) to decrease the material cost.

Received: April 25, 2012
Revised: August 13, 2012
Published online: September 23, 2012

Keywords: hydrogen · nanostructures · photosynthesis · semiconductors · water splitting

[1] M. Grätzel, *Nature* **2001**, *414*, 338 – 344.
[2] J. A. Turner, *Science* **2004**, *305*, 972 – 974.
[3] F. E. Osterloh, *Chem. Mater.* **2008**, *20*, 35 – 54.
[4] X. Chen, S. Shen, L. Guo, S. S. Mao, *Chem. Rev.* **2010**, *110*, 6503 – 6570.
[5] R. Kapadia, Z. Fan, A. Javey, *Appl. Phys. Lett.* **2010**, *96*, 103116.
[6] C. L. Pint, K. Takei, R. Kapadia, M. Zheng, A. C. Ford, J. Zhang, A. Jamshidi, R. Bardhan, J. J. Urban, M. Wu, J. W. Ager, M. M. Oye, A. Javey, *Adv. Energy Mater.* **2011**, *1*, 1040 – 1045.
[7] P. B. Clapham, M. C. Hutley, *Nature* **1973**, *244*, 281 – 282.
[8] a) Z. Fan, H. Razavi, J. Do, A. Moriwaki, O. Ergen, Y.-L. Chueh, P. W. Leu, J. C. Ho, T. Takahashi, L. A. Reichertz, S. Neale, K. Yu, M. Wu, J. W. Ager, A. Javey, *Nat. Mater.* **2009**, *8*, 648 – 653; b) Z. Fan, R. Kapadia, P. Leu, X. Zhang, Y.-L. Chueh, K. Takei, K. Yu, A. Jamshidi, A. Rathore, D. Ruebusch, M. Wu, A. Javey, *Nano Lett.* **2010**, *10*, 3823 – 3827.
[9] C. Maier, M. Specht, G. Bilger, *Int. J. Hydrogen Energy* **1996**, *21*, 859 – 864.
[10] M. A. Green, K. Emery, Y. Hishikawai, W. Warta, *Prog. Photovoltaics* **2009**, *17*, 320 – 326.
[11] Y. Hou, B. L. Abrams, P. C. K. Vesborg, M. E. Björketun, K. Herbst, L. Bech, A. M. Setti, C. D. Damsgaard, T. Pedersen, O. Hansen, J. Rossmeisl, S. Dahl, J. K. Nörskov, I. Chorkendorff, *Nat. Mater.* **2011**, *10*, 434 – 438.
[12] J. Oh, T. G. Deutsch, H.-C. Yuan, H. M. Branz, *Energy Environ. Sci.* **2011**, *4*, 1690 – 1694.
[13] S. W. Boettcher, E. L. Warren, M. C. Putnam, E. A. Santori, D. Turner-Evans, M. D. Kelzenberg, M. G. Walter, J. R. McKone, B. S. Brunschwig, H. A. Atwater, N. S. Lewis, *J. Am. Chem. Soc.* **2011**, *133*, 1216 – 1219.
[14] K. Ohashi, J. McCann, J. O. Bockris, *Nature* **1977**, *266*, 610 – 611.
[15] S. Licht, *J. Phys. Chem. B* **2001**, *105*, 6281 – 6294.
[16] C. J. Keavney, V. E. Haven, S. M. Vernon, *Conference Record, 21st IEEE Photovoltaic Specialists Conference*, Kissimimee, May, **1990**, 141 – 144.
[17] C. A. Hoffman, K. Jarašiūnas, H. J. Gerritsen, A. V. Nurmikko, *Appl. Phys. Lett.* **1978**, *33*, 536 – 539.
[18] P. G. P. Ang, A. F. Sommells, *J. Electrochem. Soc.* **1984**, *131*, 1462 – 1464.
[19] A. Heller, R. G. Vadimsky, *Phys. Rev. Lett.* **1981**, *46*, 1153 – 1156.
[20] T. Arai, S. Sato, K. Uemura, T. Morikawa, T. Kajino, T. Motohiro, *Chem. Commun.* **2010**, *46*, 6944 – 6946.
[21] See reference [7].
[22] A. Paracchino, V. Laporte, K. Sivula, M. Grätzel, E. Thimsen, *Nat. Mater.* **2011**, *10*, 456 – 461.
[23] Y. W. Chen, J. D. Prange, S. Dühnen, Y. Park, M. Gunji, C. E. D. Chidsey, P. C. McIntyre, *Nat. Mater.* **2011**, *10*, 539 – 544.
[24] J. Nelson, *The Physics of Solar Cells*, Imperial College, London, **2003**, p. 13.
[25] M. B. Spitzer, C. J. Keavney, S. M. Vernon, V. E. Haven, *Appl. Phys. Lett.* **1987**, *51*, 364.
[26] K. Shankar, J. I. Basham, N. K. Allam, O. K. Varghese, G. K. Mor, X. J. Feng, M. Paulose, J. A. Seabold, K. S. Choi, C. A. Grimes, *J. Phys. Chem. C* **2009**, *113*, 6327 – 6359.
[27] Z. Chen, T. F. Jaramillo, T. G. Deutsch, A. Kleiman-Shwarsctein, A. J. Forman, N. Gaillard, R. Garland, K. Takanabe, C. Heske, M. Sunkara, E. W. McFarland, K. Domen, E. L. Miller, J. A. Turner, H. N. Dinh, *J. Mater. Res.* **2010**, *25*, 3 – 16.
[28] I. Oh, J. Kye, S. Hwang, *Nano Lett.* **2012**, *12*, 298 – 302.
[29] J. Li, L. M. Peter, *J. Electroanal. Chem.* **1985**, *193*, 27 – 47.
[30] T. R. Hayes, U. K. Chakrabarti, F. A. Baiocchi, A. B. Emerson, H. S. Luftman, W. C. Dautremont-Smith, *J. Appl. Phys.* **1990**, *68*, 785 – 792.
[31] H. J. Lewerenz, D. E. Aspnes, B. Miller, D. L. Malm, A. Heller, *J. Am. Chem. Soc.* **1982**, *104*, 3325 – 3329.

 © 2012 Wiley-VCH Verlag GmbH & Co. KGaA, Weinheim